2D computations of 3D synthetic seismograms using the ray-based Born approximation in heterogenous model P1

Libor Šachl

Charles University, Faculty of Mathematics and Physics, Department of Geophysics,
E-mail: sachl@karel.troja.mff.cuni.cz

Summary

The accuracy of the ray-based Born approximation of the first order is tested in a smooth 2D heterogenous background model P1. Only P waves are considered. 3D synthetic seismograms are numerically calculated by the Born approximation in a 2D grid and are compared with the ray-theory seismograms. The born seismograms contain reflected and diffracted waves. Individual reflected and diffracted waves are identified.

Key words: Born approximation, ray theory, velocity model, perturbation

1 Introduction

The Born approximation is a method which allows us to use quantities computed by our chosen method, here the ray theory, in a simple background velocity model for calculating seismograms in a more complex velocity model. Let us call the background model unperturbed and the more complex model perturbed. The requirement is that the unperturbed and perturbed models are "close" to each other.

This study was motivated by synthetic seismogram computations of Bulant & Martakis (2011) in 2D heterogenous model P1I, see Section 2, using the ray theory. We wished to compute the Born seismograms in this model and compare them with Bulant's & Martakis's (2011) results. We used smooth 2D background model P1. We performed the computations, but, unfortunately, the seismograms were very different and we were unable to explain the results. Therefore we have simplified model perturbations, and study the differences between the Born and ray-theory seismograms. We calculate the 3D wavefield using the 2D Born integral according to Červený & Coppoli (1992) and Šachl (2011, eq.45)

Seismic Waves in Complex 3-D Structures, Report 21, Charles University, Faculty of Mathematics and Physics, Department of Geophysics, Praha 2011, pp. 99-114

2 Models

2.1 Background model and model perturbations

Model P1 was created by Bulant & Martakis (2011). It is a 2D velocity model situated in rectangle $(0\text{ km}, 47.3\text{ km}) \times (0\text{ km}, 6\text{ km})$. The model has two versions. The smooth version of the model should be suitable for the ray-theory computations. In our computations it serves as an unperturbed model for the ray-based Born approximation. We use the second version, model P1I, as our inspiration for the construction of simple perturbed models.

P-wave velocity v_p in smooth model P1 is depicted in Figure 1. The S-wave velocity is equal to $v_s = \frac{v_p}{\sqrt{3}}$. The density is equal to $\rho = 1000\text{ kg/m}^3$ everywhere. The Figure 1 of P-wave velocities is created using the grid which contains 4730×600 grid points. The greatest value of the discretized P-wave velocities is $(v_p)_{max} \approx 5.93\text{ km/s}$.

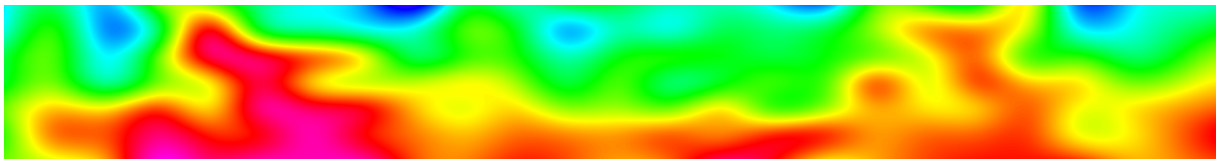

Figure 1: P-wave velocity in smooth model P1. The colour change from blue to green and red as the P-wave velocity grows.

Model P1I is quite complicated because it is composed of 16 blocks and 13 surfaces which form 15 interfaces where reflected waves may be generated. Blocks in model P1I are displayed in Figure 2. The colours are determined by the index of the block.

Figure 2: Blocks in model P1I

The greatest absolute value of the discretized P-wave perturbations is $|\Delta v_p|_{max} \approx 0.21\text{ km/s}$. See Figure 3 for the spatial distribution of the P-wave velocity perturbation and of the absolute value of the perturbation. The perturbation of S-wave velocity is not depicted, because in the models, which we constructed from model P1I, we set $v_s = \frac{v_p}{\sqrt{3}}$ analogously to the background model.

2.2 Model P1-9-homo

This is the first one of 4 perturbed velocity models we have constructed. The density is, the same as in smooth model P1, equal to $\rho = 1000\text{ kg/m}^3$ everywhere. The S-wave

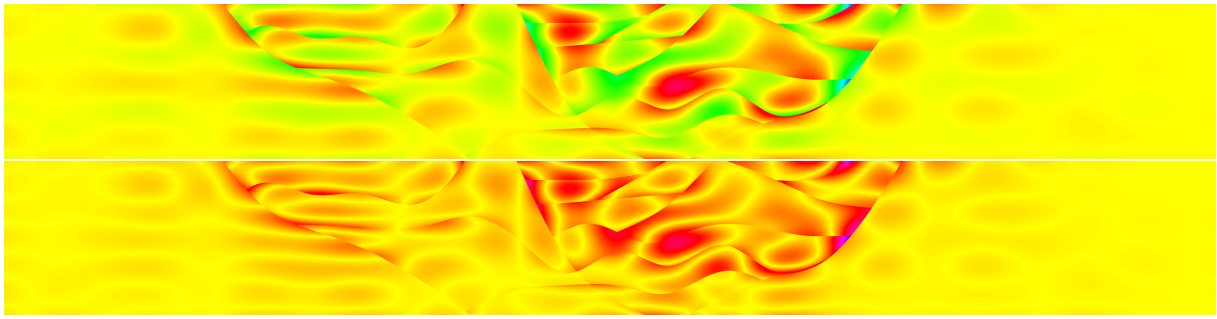

Figure 3: P-wave velocity perturbation in model P1; upper: without absolute value, lower: with absolute value. The extent of values corresponding to the whole colour circle RGB is set to 0.44 km/s. Positive perturbations are red, negative perturbations are green. Zero perturbations are drawn yellow.

velocity is related to P-wave velocity by expression $v_s = \frac{v_p}{\sqrt{3}}$. P-wave velocity is the same as in smooth model P1 except the domain which corresponds to block 9 of model P1I. Block 9 is displayed in Figure 4. The distribution of P-wave velocity in this domain is created by adding the homogenous perturbations of P-wave velocity $\Delta v_p = 0.01$ km/s to the smooth version of model P1.

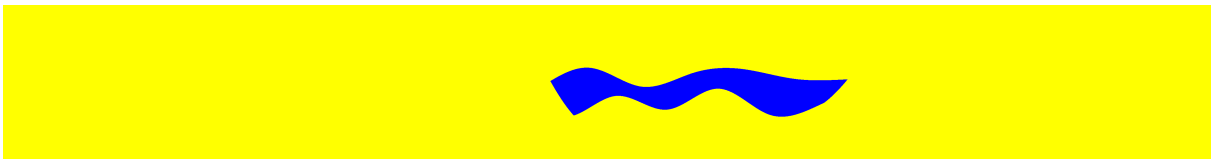

Figure 4: Block 9 in model P1I.

P-wave velocity in the unperturbed model is specified on the bicubic-spline grid containing 24×7 points (from 0 km to 46 km with step 2 km in the x_1 direction and from 0 km to 6 km with step 1 km in the x_3 direction), the values at the other points are determined by interpolation. If the grid were smaller, the values of the P-wave velocities would be different, even in the interior points. With the view of sidetracking this behaviour we specified P-wave velocity in block 9 on the same grid of 24×7 points.

2.3 Model P1-9-10%

Everything, what we wrote about model P1-9-homo applies to model P1-9-10% except for the P-wave velocity in block 9. The distribution of P-wave velocity in this domain is constructed as a linear combination of the distribution in smooth model P1 and model P1I:

$$v_p = 0.9(v_p)_{unperturbed} + 0.1(v_p)_{perturbed}. \tag{1}$$

2.4 Model P1-8-10%

This model is similar to model P1-9-10%, but the perturbation (1) of P-wave velocity is applied to block 8 rather than block 9. Block 8 is depicted in Figure 5.

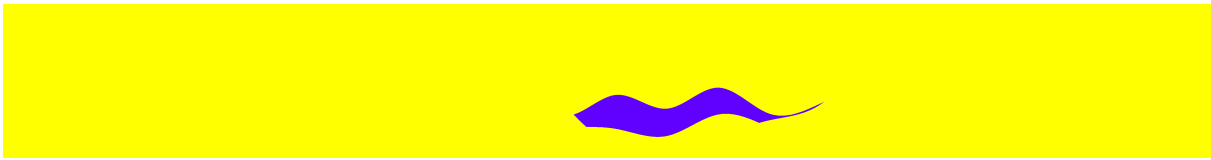

Figure 5: Block 8 in model P1I.

2.5 Model P1-8&9-10%

In this velocity model, P-wave velocity perturbation (1) is applied to both blocks 8 and 9.

3 2D computations of 3D seismograms

In all numerical examples we compute the ray-theory seismograms using once reflected P waves and compare them with the ray-based Born approximation of the first order. Only P waves are considered. The receiver is at point (16 km, 0 km, 0 km), the source is at point (25 km,0 km,0 km).

3.1 Shooting rays

First of all, it was necessary to decide how to shoot the rays. Bulant & Martakis (2011) shot rays in the angular interval $\langle -1.4, 1.4\rangle$ radians, where zero corresponds to a ray shot downwards, $-\frac{\pi}{2}$ to a ray shot horizontally to the left and $\frac{\pi}{2}$ to a ray shot horizontally to the right. He thus did not shoot rays into the whole lower half-plane. The reason is that otherwise he would calculate the direct wave as well, despite the fact that he is interested in the once reflected waves only. But when using the Born approximation we shoot rays in the unperturbed medium, therefore we have just direct waves and we wish to cover the whole model with the ray tubes. The ray tubes cannot be "too wide", because quantities on the specified grid are calculated by interpolation within them. Bulant & Martakis (2011) covered the angle, into which he shot the rays, by 11 rays. This basic system of rays is sufficient for two point ray tracing, but probably insufficient for controlled initial value ray tracing, which we are interested in. Focusing on these two aspects we tried several basic systems of rays. We shot rays from the position of the source into interval $\langle -1.57, 1.57\rangle$ covering nearly the whole lower half-plane, but from the position of the receiver we kept the original option $\langle -1.4, 1.4\rangle$. We tried basic systems of rays composed of 11, 21, 46, 91, 121 rays for the rays shot from the position of the source. We tried basic systems of rays composed of 11, 21, 46, 91, 121 rays for the rays shot from the position of the receiver. We propose to use interval $\langle -1.57, 1.57\rangle$ and 91 basic rays when shooting from the position of the source, see Figures 6 and 7. We propose to use interval $\langle -1.4, 1.4\rangle$ and 91 basic rays when shooting from the position of the receiver, see Figures 8 and 9.

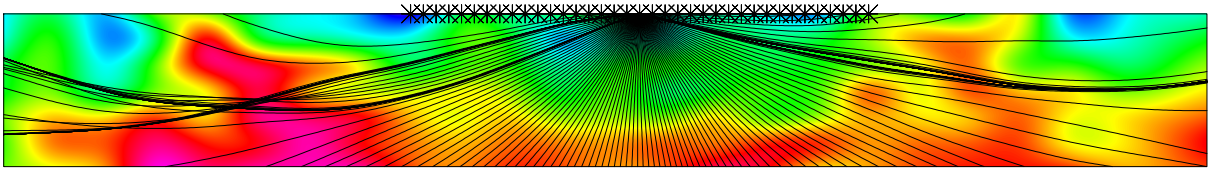

Figure 6: Coverage of smooth model P1 with the rays when shooting from the position of the source. Background: P-wave velocity.

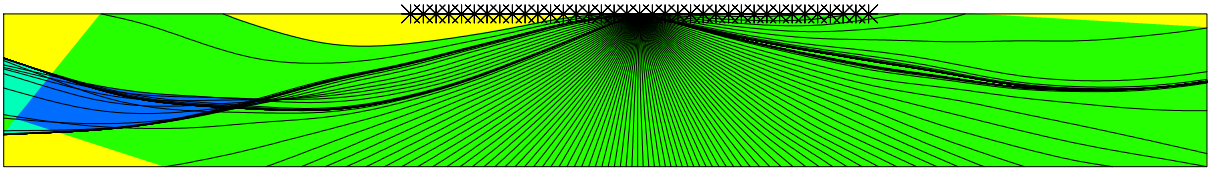

Figure 7: Coverage of smooth model P1 with the rays when shooting from the position of the source. Background: numbers of arrivals.

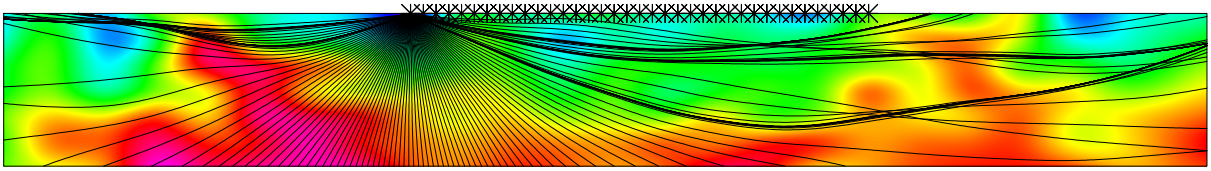

Figure 8: Coverage of smooth model P1 with the rays when shooting from the position of the receiver. Background: P-wave velocity.

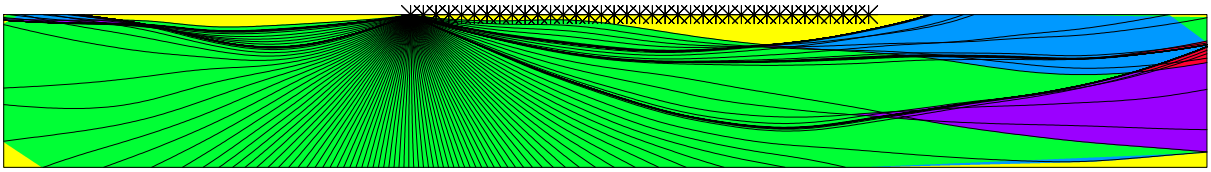

Figure 9: Coverage of smooth model P1 with the rays when shooting from the position of the receiver. Background: numbers of arrivals.

3.2 Model P1-9-homo

In the SW3D programs, the following specification of the grid is used: O_1, O_2, O_3 are the coordinates of the origin of the grid. N_1, N_2, N_3 are the numbers of gridpoints along the x_1, x_2, x_3 coordinate axes, and D_1, D_2, D_3 are the grid intervals in the directions of the x_1, x_2, x_3 coordinate axes. We use this notation also in this paper.

The minimum P-wave velocity at the grid points is equal to $(v_p)_{min} = 4.65235$ km/s (the maximum is $(v_p)_{max} = 5.91815$ km/s). In the 2D models, which we previously used, see Šachl (2011), the used grids had the smallest value of the grid interval in the vertical direction. The best values of the vertical grid interval were $D_3 = 0.025$ km in model 1, $D_3 = 0.017489$ km in model 2 and $D_3 = 0.00625$ km in model 3. If we recalculate these values using $(v_p)_{min}$ we acquire values $D_3 = 0.019$ km, $D_3 = 0.014$ km

and $D_3 = 0.0048$ km, respectively. Therefore we choose grid intervals $D_1 = 0.005$ km, $D_3 = 0.005$ km.

Note that a grid, which covers the whole model is superfluously big for the computation of the Born approximation, because perturbations are nonzero only in block 9. In the case of model p1-9-homo, we use a smaller grid, given by parameters $N_1 = 2500$, $D_1 = 0.005$ km, $O_1 = 21.0025$ km, $N_3 = 500$, $D_3 = 0.005$ km, $O_3 = 2.005$ km, and covering the part of the model displayed in Figure 10.

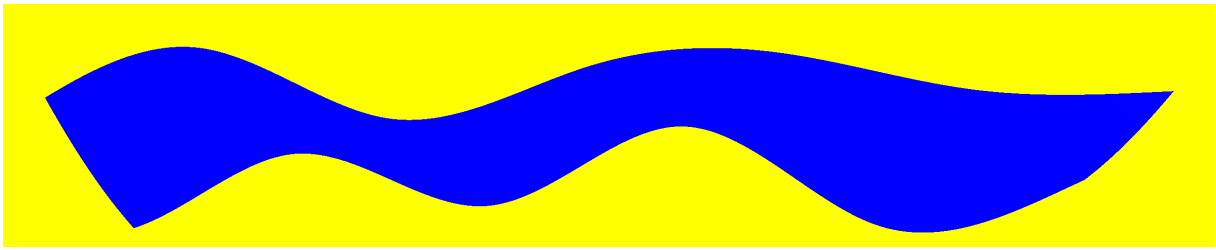

Figure 10: Small grid with 2500×500 points used in the computations with block 9 covers only the displayed part of model P-9-homo from Figure 13.

After applying all discussed options and parameters, we calculate the seismogram displayed in Figure 11. The seismogram contains 2 reflected waves computed by the ray theory, as you can see from Figure 13. The ray reflected from the upper interface arrives first, at approximately 2.06 s. The ray reflected from the lower interface arrives, as one would expect, later, at approximately 2.93 s. The agreement between the Born and ray-theory seismograms is not bad, but there are some discrepancies and we are interested in the reasons of difference. We thus subtracted the ray-theory seismogram from the Born seismogram, see Figure 12. The abscissae in Figures 11 and 12 are travel times which correspond to the waves diffracted from 4 edges of block 9. The travel times of the individual diffracted wave are given by Table 1, where each diffracted wave is described by the edge, from which it is diffracted. In Figures 14, 15, 16 and 17, we see the isochrones

Edge	left upper	left lower	right upper	right lower
Travel time [s]	2.12	2.45	5.05	4.80

Table 1: The travel times of the waves diffracted from the edges of block 9

of travel times which correspond to travel times of these diffracted waves. We think that the major discrepancies can be explained by the absence of the diffracted waves in the ray-theory seismogram. Note that, to determine the travel time of the diffraction, we firstly make a rough guess of the position of the edge from Figure 2. The numbers of blocks at the dense rectangular grid centered to our guessed position are computed. The edge is determined using this grid, with the discretization error of the order of D_1. The position of the edge is entered into the computation of isochrone with the precision of 2 decimal places.

If the P-wave perturbation is small and homogenous, we are able to compare both seismograms and we think that we more or less know what cause the differences. But in the original version of P1 model, the perturbations are bigger, see Section 2.1. It

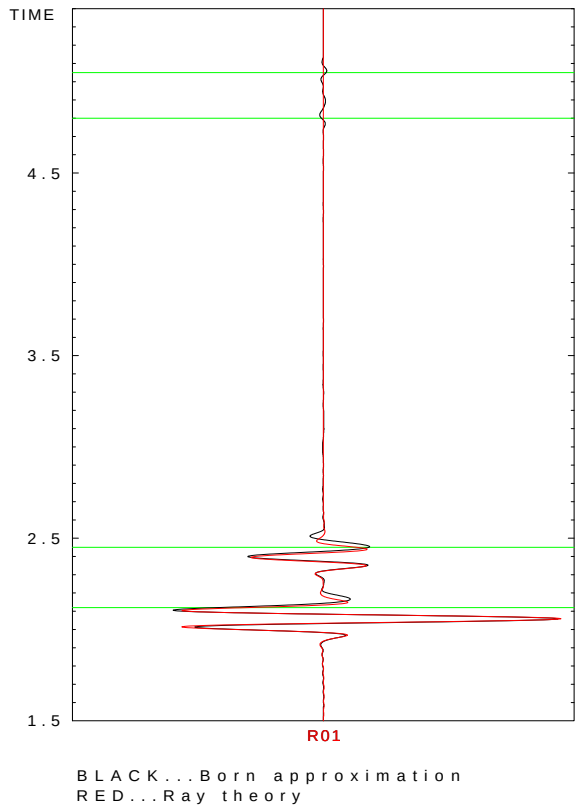

Figure 11: Model P1-9-homo, grid with grid intervals 0.005 km × 0.005 km.

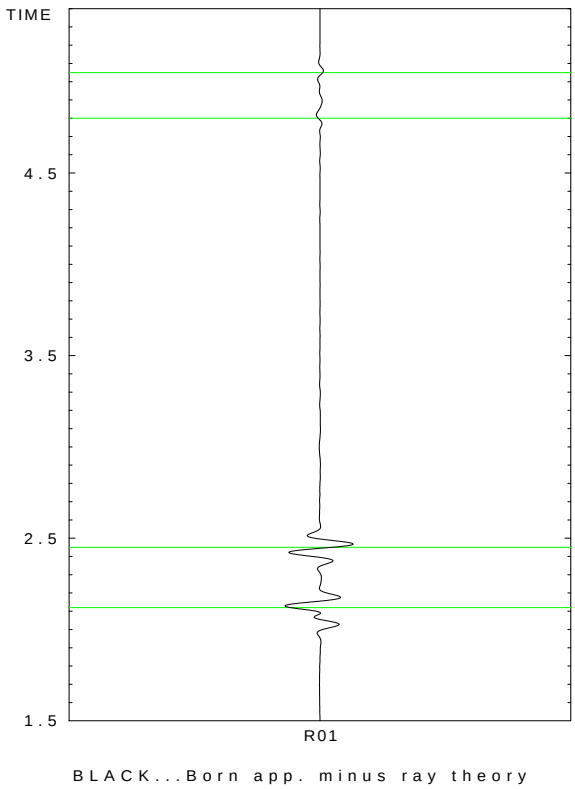

Figure 12: Model P1-9-homo, grid intervals 0.005 km × 0.005 km, the Born seismogram minus the ray-theory seismogram.

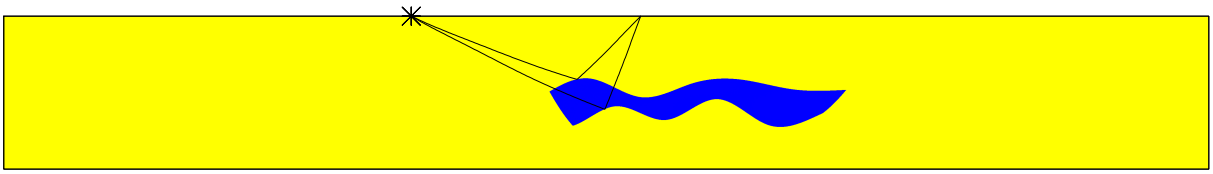

Figure 13: The reflected rays in model P1-9-homo.

is therefore necessary to acquire insight into how much can perturbations be increased without loss of precision. We tested values of P-wave velocity perturbations 0.02 km/s, 0.04 km/s, 0.08 km/s, 0.1 km/s, 0.2 km/s and 0.3 km/s. The results are shown only for 0.02 km/s, 0.1 km/s, 0.2 km/s and 0.3 km/s, see Figures 18, 19, 20 and 21, where the time window is shortened in order to see the effect better. The figures are scaled with respect to the greatest value in the ray-theory seismogram to compare them easily. In case of the first wave, reflected from the upper interface, the discrepancies in amplitude grow. In case of the second wave this happens too, but moreover we observe time shift. The reason is that there are no perturbations of material parameters (except the interface itself) along the path of the first ray, whereas the perturbations in block 9 are present along the path of the second ray. We see that we cannot magnify the perturbations too much. If we take the greatest value in the seismogram computed using the Born approximation for P-wave velocity perturbations equal to 0.01 km/s and perform a linear prediction with respect to the perturbations, which matches the behavior of the Born approximation, we obtain the blue curve in Figure 22. But the ray-theory result is a bit different, see the red points.

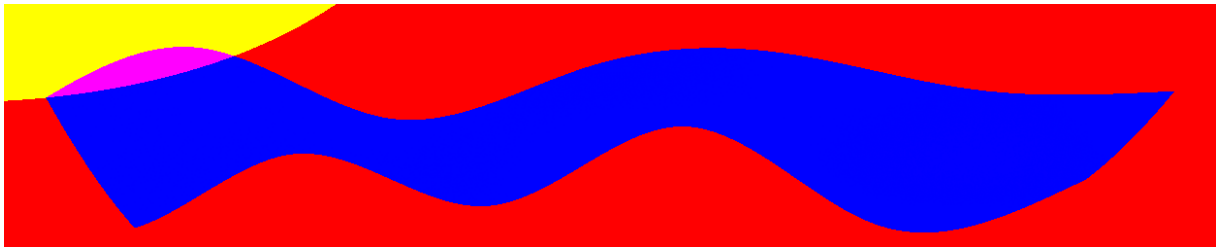

Figure 14: Isochrone of travel time 2.12 s in unperturbed model P1.

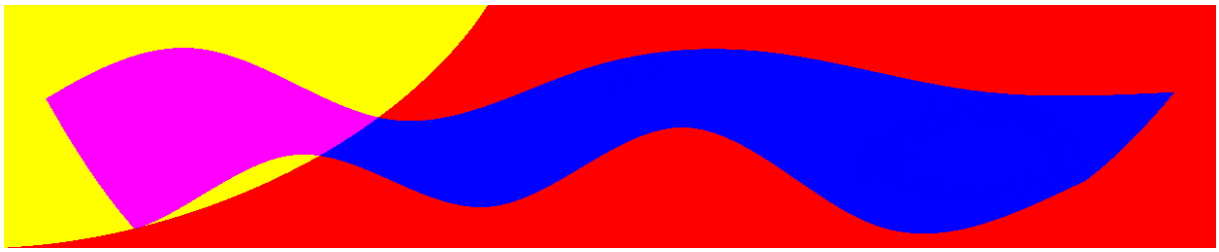

Figure 15: Isochrone of travel time 2.45 s in unperturbed model P1.

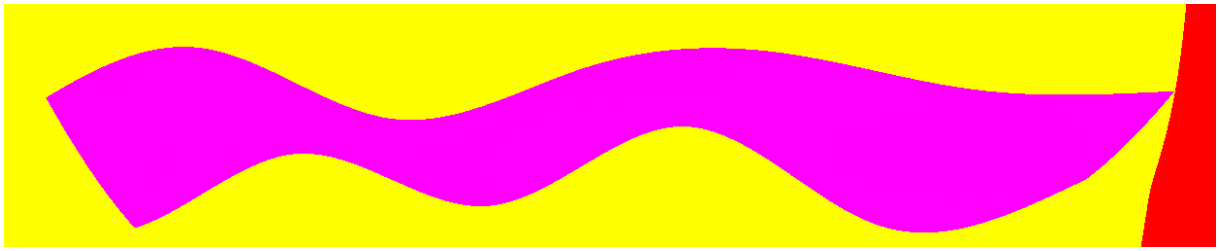

Figure 16: Isochrone of travel time 5.05 s in unperturbed model P1.

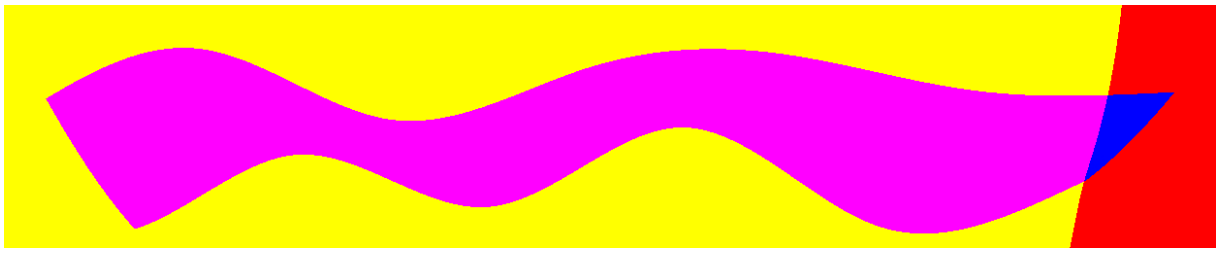

Figure 17: Isochrone of travel time 4.80 s in unperturbed model P1.

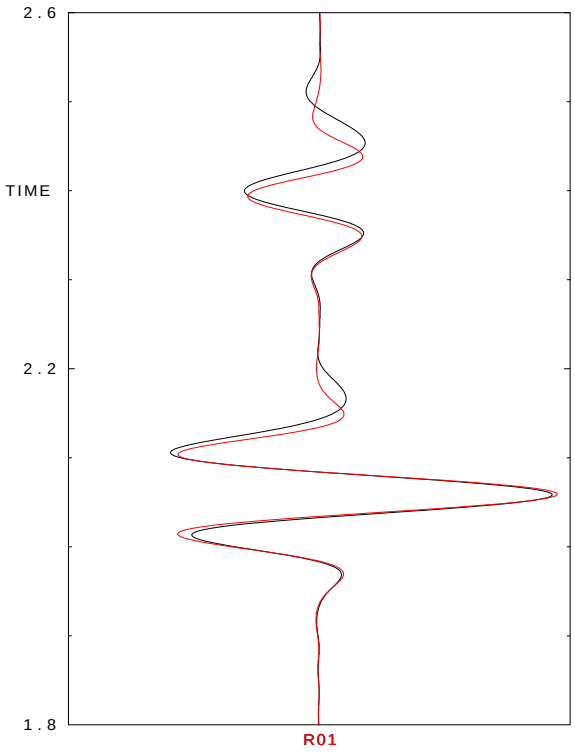

Figure 18: Model P1-9-homo, grid intervals 0.005 km × 0.005 km, $\Delta v_p = 0.02$ km/s

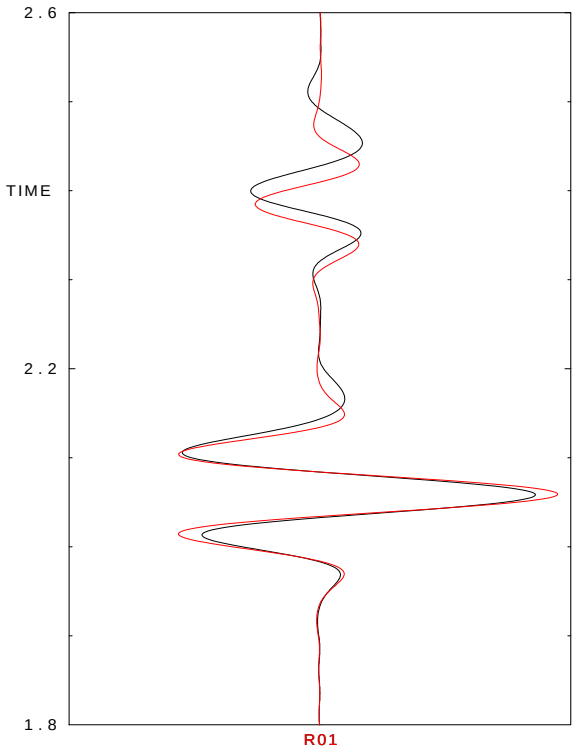

Figure 19: Model P1-9-homo, grid intervals 0.005 km × 0.005 km, $\Delta v_p = 0.1$ km/s

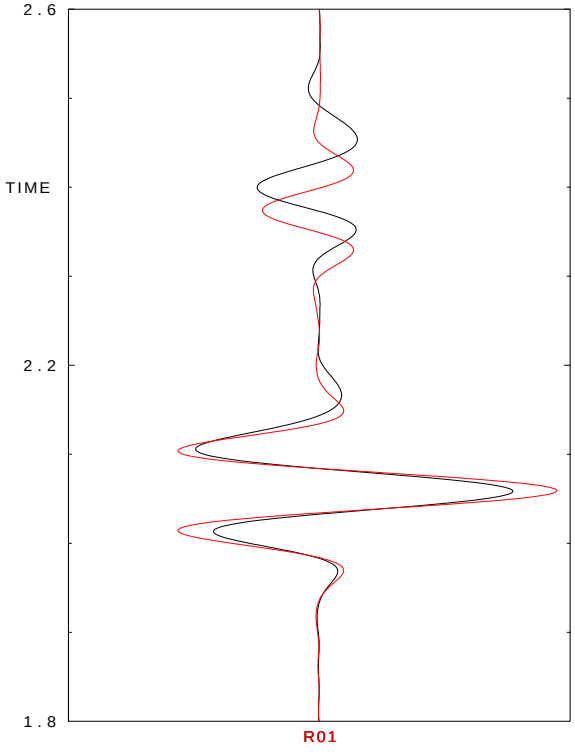

Figure 20: Model P1-9-homo, grid intervals 0.005 km × 0.005 km, $\Delta v_p = 0.2$ km/s

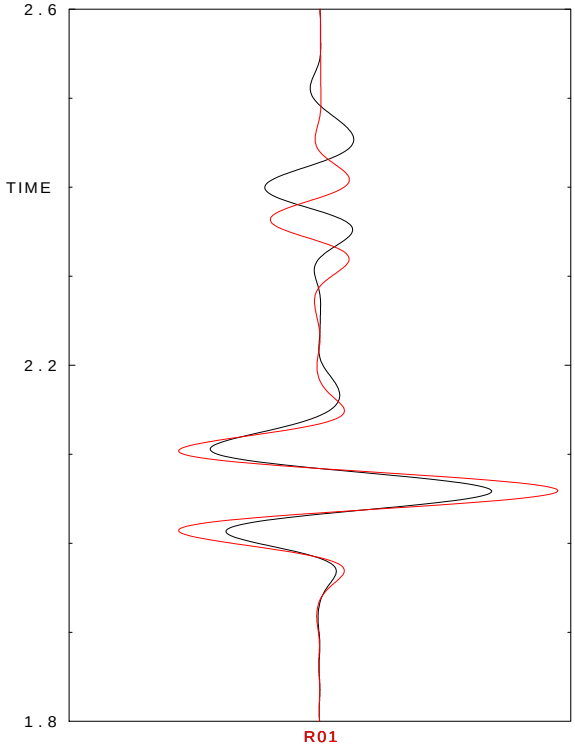

Figure 21: Model P1-9-homo, grid intervals 0.005 km × 0.005 km, $\Delta v_p = 0.3$ km/s

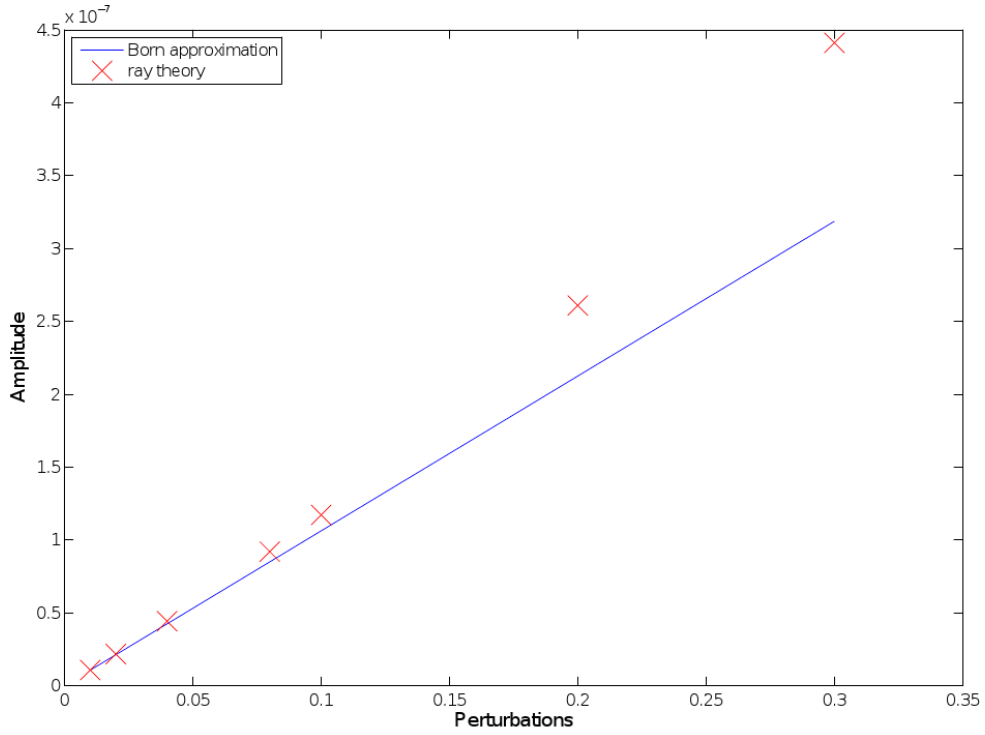

Figure 22: Maximum amplitudes in the Born and ray-theory seismograms for growing perturbations.

We conclude that it is a consequence of nonlinearity of the reflection coefficient, because the greatest value in the seismogram belongs to the reflection from the upper interface. In principle, we see its Taylor expansion with respect to the perturbations. Only the linear term is important for very small values, further the quadratic term plays the role and so on. Table 2 summarizes the relative amplitude difference ΔA between the ray-theory amplitude A_{rt} and the Born amplitude A_{Ba}. The formula for ΔA reads

$$\Delta A = \frac{A_{rt} - A_{Ba}}{A_{Ba}} 100\%. \tag{2}$$

Δv_p [km/s]	0.01	0.02	0.04	0.08	0.1	0.2	0.3
ΔA [%]	1.22	2.17	4.10	8.19	10.36	22.79	38.42

Table 2: The evolution of the relative amplitude difference ΔA with respect to the P-wave velocity perturbations.

3.3 Model P1-9-10%

From what was shown and said we worried about the usage of model P1I because the maximum measured perturbations were $|\Delta(v_p)|_{max} \approx 0.21$ km/s and Figure 20 has some

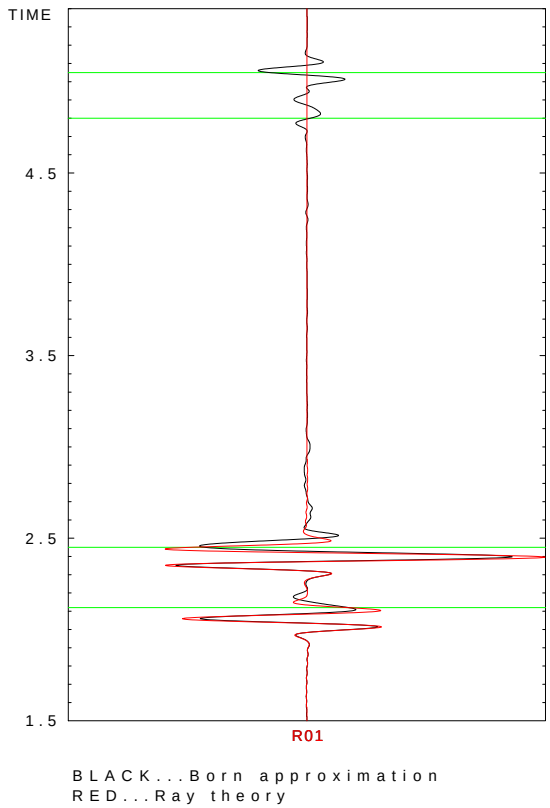

Figure 23: Model P1-9-10%, grid intervals 0.005 km × 0.005 km

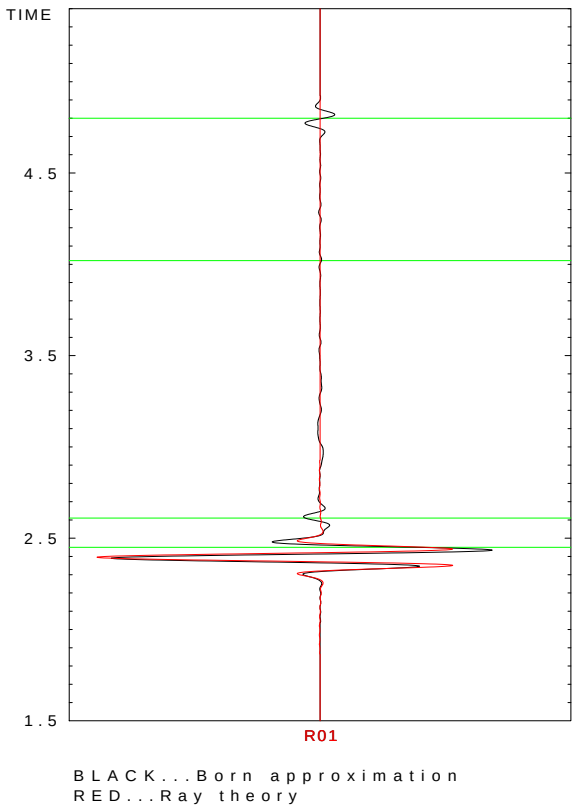

Figure 24: Model P1-8-10%, grid intervals 0.005 km × 0.005 km

problems. Therefore we prepared a model with suitably low perturbations, see Sec. 2.3. The perturbations in this model are ten times smaller compared to the original model P1I. With regard to Figure 18 it seems sufficient.

We obtained seismograms displayed in Figure 23. The differences between the Born and ray-theory seismograms are bigger in Figure 23 than in case with the homogenous perturbation displayed in Figure 11. Nevertheless, the drawn diffractions play role again. We see that the differences between seismograms appear in both wavegroups at higher times.

3.4 Model P1-8-10%

The Born seismogram computed in this model is compared with the ray-theory seismogram in Figure 24. Similarly to the previous cases, the times of diffracted waves are computed and marked. The travel times of the individual diffracted waves are given by Table 3. There is only one reflected wave, see Figure 25, but the displayed features are common with the previous example.

Edge	left upper	left lower	right upper	right lower
Travel time [s]	2.45	2.61	4.80	4.02

Table 3: The travel times of the waves diffracted from the edges of block 8

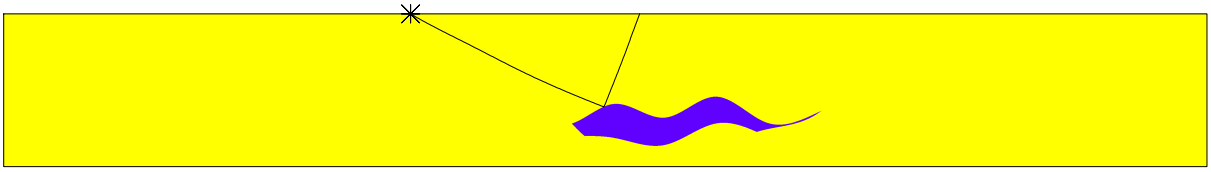

Figure 25: The reflected ray in model P1-8-10%

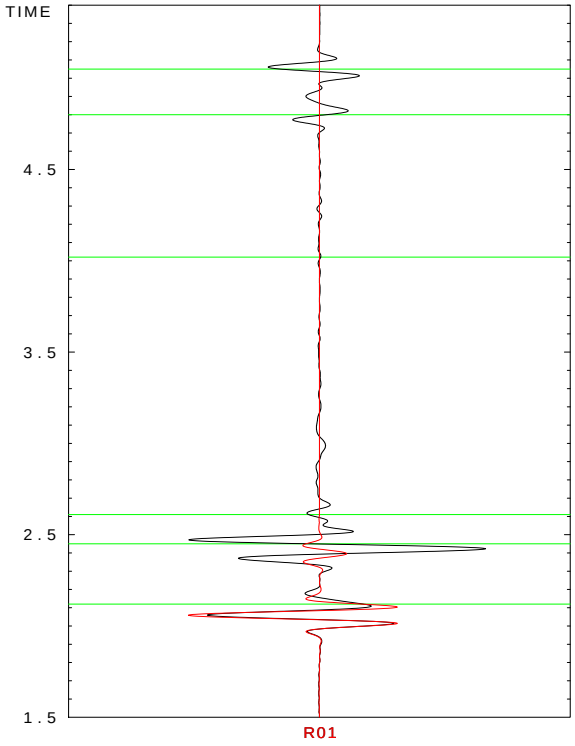

Figure 26: Model P1-8&9-10%, grid intervals 0.005 km × 0.005 km

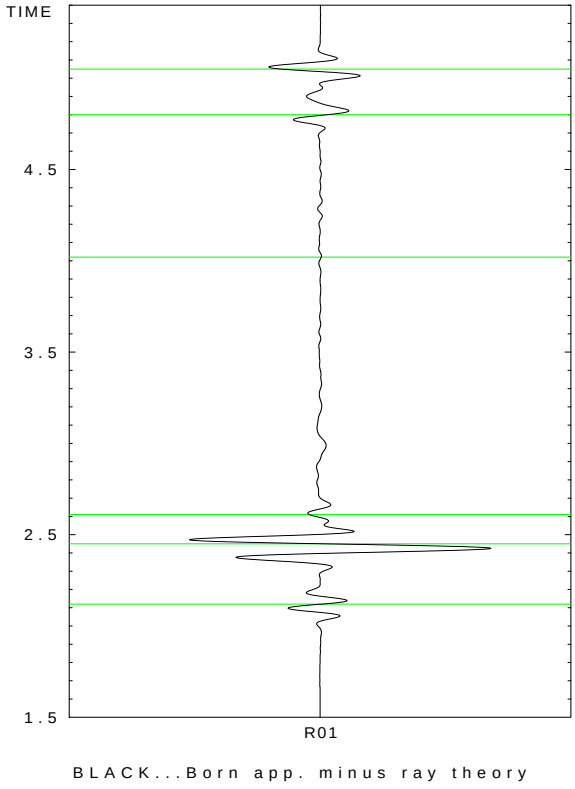

Figure 27: Model P1-8&9-10%, grid intervals 0.005 km × 0.005 km, the Born seismogram minus the ray-theory seismogram

3.5 Model P1-8&9-10%

In this computation, we applied perturbations to both block 8 and block 9. The travel times of the individual diffracted waves are given by Table 4. Considering the separate

Edge	left upper	left middle	left lower	right upper	right middle	right lower
Travel time [s]	2.12	2.45	2.61	5.05	4.80	4.02

Table 4: The travel times of the waves diffracted from the edges of block 8 and block 9

computations in these blocks, we expect to obtain seismogram similar to the ray-theory result. Figure 26 is therefore quite a surprise. There is a significant discrepancy in

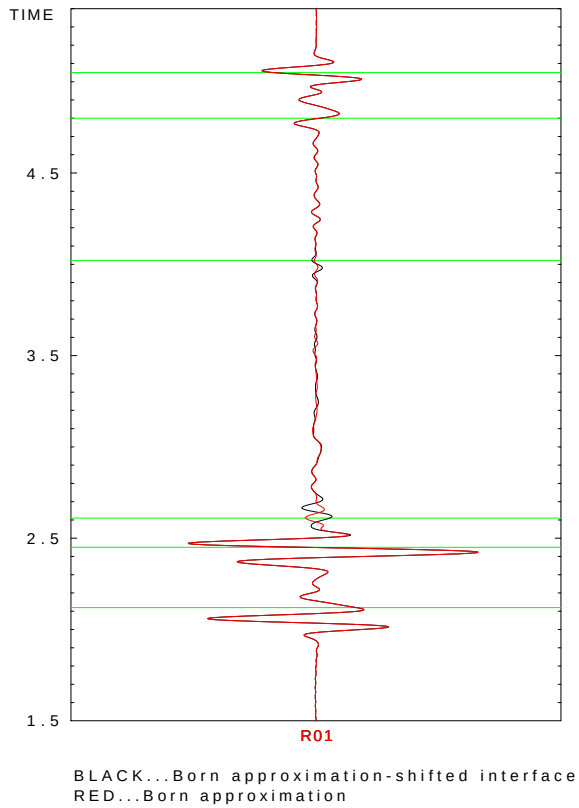

Figure 28: Model P1-8&9-10%, grid intervals 0.01 km × 0.01 km, $\frac{\lambda}{4}$ shift of the lower interface

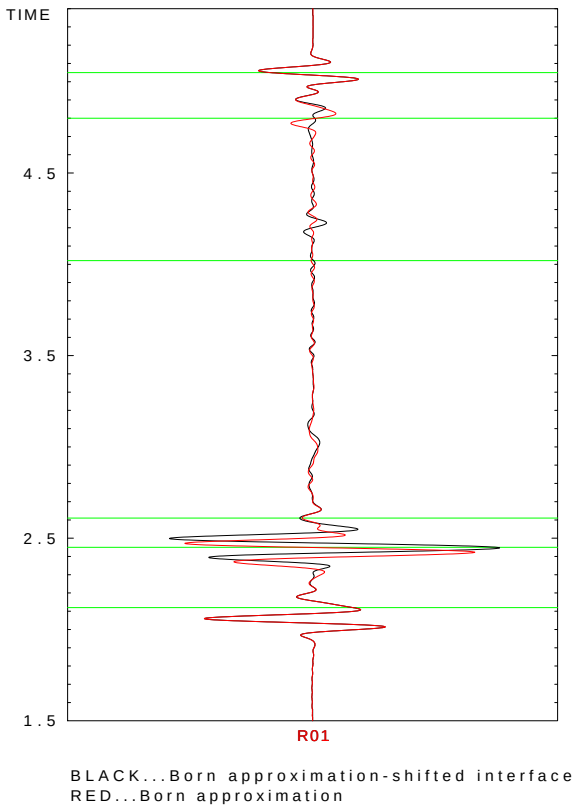

Figure 29: Model P1-8&9-10%, grid intervals 0.01 km × 0.01 km, $\frac{\lambda}{4}$ shift of the middle interface

the second wavegroup. To see the discrepancy precisely we subtracted the ray-theory seismogram from the Born seismogram, see Figure 27. Now it appears that the difference is again caused by diffraction but why is it so strong?

In order to get some hint we tried to slightly ($\frac{\lambda}{4}$) shift each of 5 interfaces (4 outer and one between blocks). Left interface was shifted to the right, right to the left and lower, middle and upper interface downwards. These computations use coarser grid which covers the whole model volume with grid intervals $D_1 = D_2 = 0.01$ km. We want to study shifts of waves on the seismogram, therefore it should not interfere our conclusions. Let us observe Figures 28, 29, 30, 31 and 32. The first wavegroup marked by abscissa in 2.12 reacts to the shift of the middle interface, because it is the reflection from this interface. The first wavegroup is also sensitive to the shift of the left interface, we observe signal deformation. This sensitivity is caused by the diffracted wave superposed with the reflected wave. Similarly, the second wavegroup marked by abscissa in 2.45 s is sensitive to the shift of the middle and left interface. The wave marked by abscissa in 2.61 s is sensitive to the shift of the lower and left interface. The wave marked by abscissa in 4.02 s is sensitive to the shift of the lower interface and it should be sensitive to the shift of the right interface but this is not apparent. Two significant waves at the end of the seismogram are sensitive to the shift of the right interface. The wave marked by abscissa in 4.80 s is sensitive to the shift of the middle interface. The wave marked by abscissa in 5.05 s is sensitive to the shift of the upper interface.

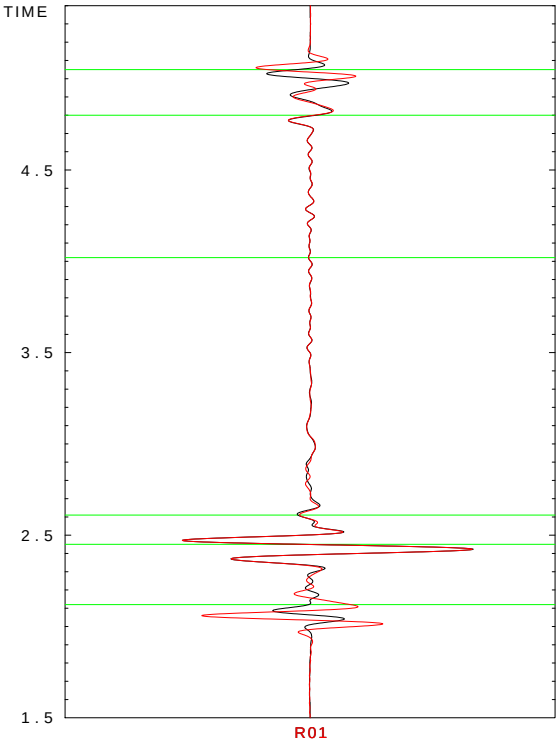

BLACK...Born approximation-shifted interface
RED...Born approximation

Figure 30: Model P1-8&9-10%, grid intervals 0.01 km × 0.01 km, $\frac{\lambda}{4}$ shift of the upper interface

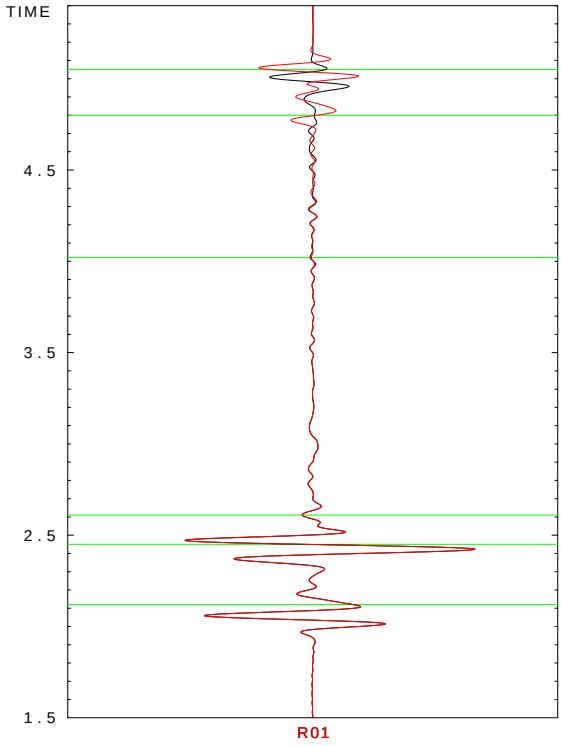

BLACK...Born approximation-shifted interface
RED...Born approximation

Figure 31: Model P1-8&9-10%, grid intervals 0.01 km × 0.01 km, $\frac{\lambda}{4}$ shift of the right interface

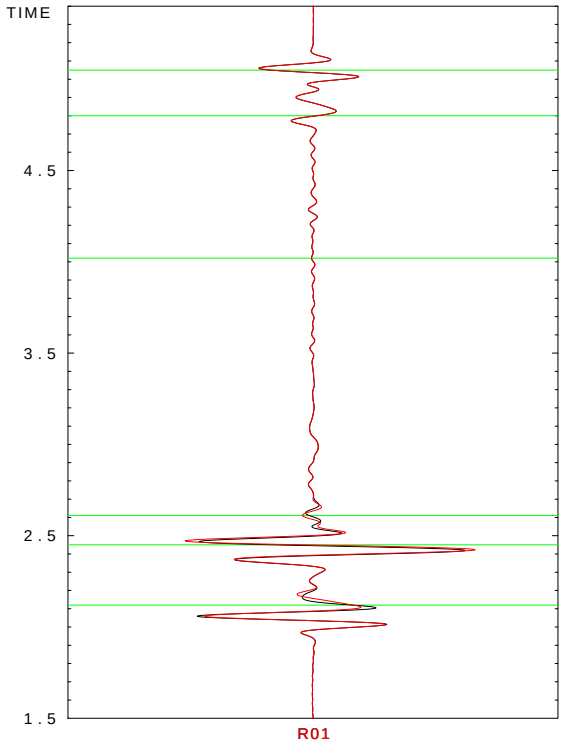

BLACK...Born approximation-shifted interface
RED...Born approximation

Figure 32: Model P1-8&9-10%, grid intervals 0.01 km × 0.01 km, $\frac{\lambda}{4}$ shift of the left interface

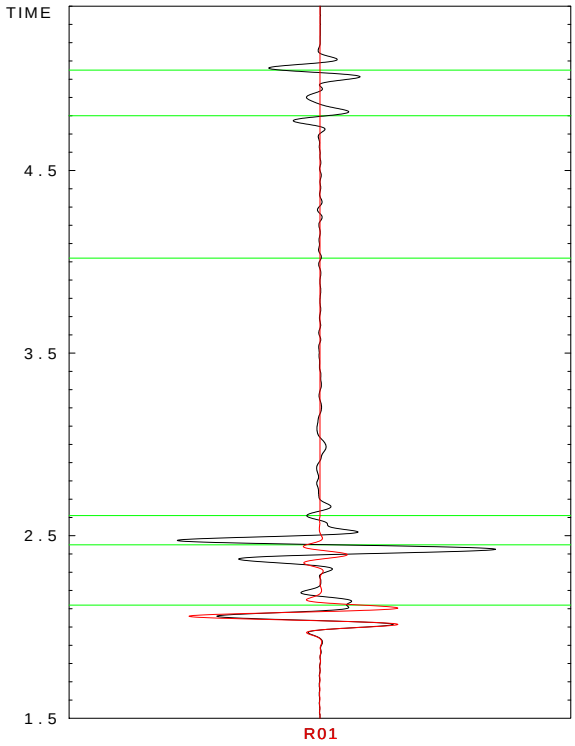

BLACK...Born approximation
RED...Ray theory

Figure 33: Model P1-8&9-10%, grid intervals 0.005 km × 0.005 km, shift 0.1 km of the left interface to the left

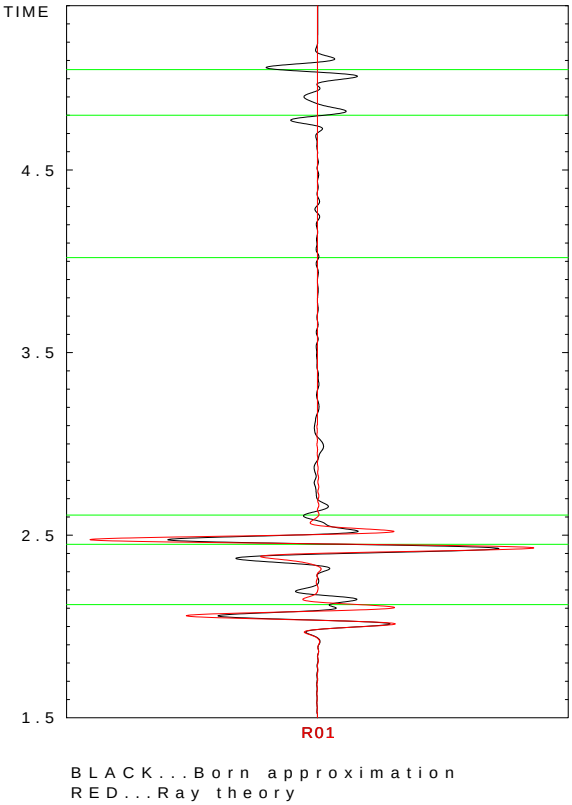

Figure 34: Model P1-8&9-10%, grid intervals 0.005 km $\times$ 0.005 km, shift 0.15 km of the left interface to the left

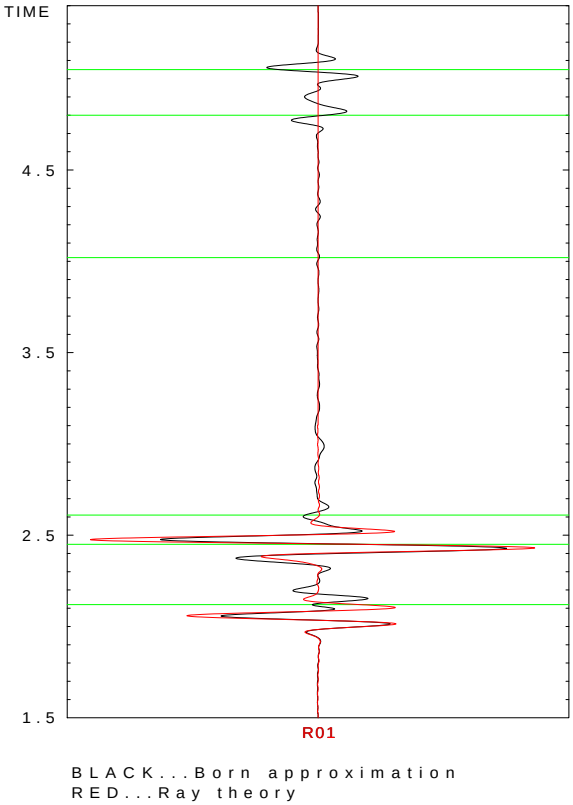

Figure 35: Model P1-8&9-10%, grid intervals 0.005 km $\times$ 0.005 km, shift 0.2 km of the left interface to the left

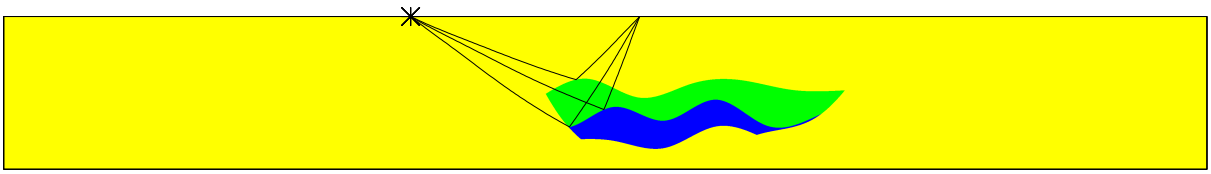

Figure 36: The reflected rays in model P1-8&9-10% with left interface shifted by 0.15

This motivated us to shift the left interface not only rightwards but also leftwards with shift values 0.1 km, 0.15 km and 0.2 km, the corresponding seismograms are displayed in Figures 33, 34 and 35. One thing is obvious. A very dramatic change of the ray-theory seismogram occurs when increasing the shift from 0.1 km to 0.15 km. Figure 36 demonstrates that there arises a new reflected ray. From the ray-theory point of view this change is immediate, but in the Born approximation this process is different. The diffraction contains the reflection and grows gradually. For this reason the diffraction is so strong. In addition, we observe that the first wavegroup is really composed of 2 waves. Their separation is apparent and grows, because the reflected wave does not change its position, while the diffracted wave does.

4 Concluding remarks

In this paper we compared the seismograms of once reflected waves computed by the ray theory with seismograms obtained by the ray-based first-order Born approximation. Both unperturbed and perturbed models are heterogenous and isotropic. We observed differences between seismograms computed by the two mentioned methods. The differences are caused by several aspects:

(a) The absence of the diffracted waves in the ray-theory seismograms.

(b) The Born approximation breaks down if the perturbations of medium parameters are too big. One of the reasons is that the Born approximation is linear with respect to medium perturbations while the reflection coefficient is nonlinear. Another one is the time shift in the Born seismograms, because they are computed in the unperturbed medium.

(c) If a ray is reflected from an interface close to the edge of the interface, a next close ray need not be reflected and the refflected wave suddenly disapears from the ray-theory seismogram. In the Born seismogram, the wave diffracted at the edge provides a smooth transition from the reflected wave to the shadow.

Acknowledgements

First of all I would like to thank Luděk Klimeš, who greatly helped me with the work which led to this paper. I would also like to thank Petr Bulant because he provided me model P1 and the history files, which he used for seismogram computation and visualization of the medium parameters. Hence if I wanted to compute the reference seismogram or to visualize some quantities I used parts of these history files (or the whole history files) and adjusted them as necessary.

The research has been supported by the Grant Agency of the Czech Republic under contract P210/10/0736, by the Ministry of Education of the Czech Republic within research project MSM0021620860, and by the members of the consortium "Seismic Waves in Complex 3-D Structures" (see "http://sw3d.cz").

References

Bulant, P. & Martakis, N. (2011): Constructing model P1I for reflection studies. In: *Seismic Waves in Complex 3–D Structures, Report 21*, pp. 17-26, Dep. Geophys., Charles Univ., Prague.

Červený V. & Coppoli A. D. M. (1992): Ray-Born synthetic seismograms for complex structures containing scatterers. In: *Journal of seismic exploration 1, 191-206.*

Šachl, L. (2011): 3D and 2D computations of 3D synthetic seismograms using the ray-based Born approximation in simple models. In: *Seismic Waves in Complex 3–D Structures, Report 21*, pp. 69-98, Dep. Geophys., Charles Univ., Prague.